International Journal of Minerals, Metallurgy and Materials
Volume 17, Number 5, October 2010, Page 526
DOI: 10.1007/s12613-010-0353-1

Estimation of froth flotation recovery and collision probability based on operational parameters using an artificial neural network

Saeed Chehreh Chelgani[1)], *Behzad Shahbazi*[2)], *and Bahram Rezai*[3)]

1) Surface Science Western, Research Park, University of Western Ontario, London Ont. N6G 0J3, Canada

2) Mining Engineering Department, Science and Research Branch, Islamic Azad University, Tehran 1477893855, Iran

3) Amirkabir University of Technology, Tehran 158754413, Iran

(Received: 19 October 2009; revised: 23 November 2009; accepted: 17 December 2009)

Abstract: An artificial neural network and regression procedures were used to predict the recovery and collision probability of quartz flotation concentrate in different operational conditions. Flotation parameters, such as dimensionless numbers (Froude, Reynolds, and Weber), particle size, air flow rate, bubble diameter, and bubble rise velocity, were used as inputs to both methods. The linear regression method shows that the relationships between flotation parameters and the recovery and collision probability of flotation can achieve correlation coefficients (R^2) of 0.54 and 0.87, respectively. A feed-forward artificial neural network with 3-3-3-2 arrangement is able to simultaneously estimate the recovery and collision probability as the outputs. In testing stages, the quite satisfactory correlation coefficient of 0.98 was achieved for both outputs. It shows that the proposed neural network models can be used to determine the most advantageous operational conditions for the expected recovery and collision probability in the froth flotation process.

Keywords: flotation; recovery; collision; probability; neural networks

1. Introduction

Derjaguin and Dukhin were the first to describe bubble-particle interactions in flotation by considering surface forces. They considered that, before adhering on the surface of an air bubble, the particles must pass through three distinct zones, hydrodynamic, diffusiophoretic, and wetting zones [1].

The primary aim in flotation is the selective attachment of hydrophobic particles to air bubbles under dynamic conditions (agitation, mixing, and vortex formation) generated by the action of an impeller when the process is carried out by mechanical cells. Therefore, it is useful to consider the extent of hydrodynamic parameters which influence the flotation performance, since they play a major role in particle/bubble collision, attachment, and transport within an environment that hold some degree of turbulence [2-4]. The influences of some dimensionless hydrodynamic parameters, such as Reynolds number (*Re*), Froude number (*Fr*), and Weber number (*We*), on the microflotation performance of quartz coarse particles were studied in this paper.

Besides surface forces, hydrodynamic interaction also plays a very important kinetic role in determining the collision efficiency between particles, the state of particulate suspension, and flotation. The extent of the hydrodynamic effect is determined by the character of the liquid field flowing around the particles, which is dependent on the type of flow in turn, *i.e.*, the Reynolds number. Hydrodynamic forces influence the rates of aggregate growth and breakup in several ways [5-9]. Bubble-particle capture is the very heart of the froth flotation process for the selective flotation of mineral particles. In addition, bubble-particles are produced as a result of a comminuting process, which inevitably produces a distribution of particle sizes. The bubble-particle capture process is clearly of key interest to the mineral processor, each particle possesses a flotation rate constant that reflects, in part, both the particle size and the degree of hydrophobicity. There have been a few successful

Corresponding author: Saeed Chehreh Chelgani E-mail: Sos4552@gmail.com

attempts to link the latter quantities in a coherent manner [10].

Artificial neural network (ANN) modeling is essentially a 'black box' operation, linking input to output data and using a particular set of nonlinear basis functions. ANNs consist of simple synchronous processing elements, which are inspired by biological nervous systems [11]. The basic unit in ANN is the neuron [12]. ANNs are the powerful tool and have been applied successfully in numerous fields of mineral processing, for example, the prediction of coal microbial and chemical desulphurization [13-15], Al_2O_3 leaching recovery in the Bayer process [16], and coal Hargrove grindability index [17-18].

Flotation is one of the processes for which ANNs can be utilized with great benefit. The multiplicity of factors to be taken into consideration in the flotation process complicates any modeling using classical statistical techniques. Cilek predicted the locked cycle flotation test by use of neural networks, and Labidi *et al.* used neural networks to predict the effect of operational parameters on the efficiency of ink removal from paper by flotation [19-20]. They found that the neural network model can be used to accurately determine the optimal operational conditions.

In this work, the regression and ANN predictions of recovery and collision probability in quartz flotation were based on the dimensionless parameters (such as Froude number, Reynolds number, and Weber number), particle size, air flow rate, bubble diameter, and bubble rise velocity. The main aim of the present study is to assess whether it is possible to use experimental data to predict the recovery and collision probability of quartz froth flotation by means of neural networks and regression. To the authors' knowledge, this is the first time that ANNs have been used to predict both recovery and collision probability in the froth flotation process.

2. Experimental

Flotation experiments were carried out using coarse quartz particles in four diameter classes (–300+212, –420+300, –500+420, and –590+500 μm). The chemical composition of the sample is given in Table 1.

The most extensively used types of anionic collectors are long-chain fatty acids and their salts, especially oleic acid or its soap, sodium oleate. Almost 100% of the fatty acids used in ore flotation are derived from tall oil, a by-product of the paper industry. Additionally, the sensitivity of fatty acids to slimes and ions in the flotation cell, the higher temperature requirement, and the relatively high consumption alternative sources of surfactants are under investigation [21].

Table 1. Chemical composition of quartz used in the experiments **wt%**

SiO_2	98.83
CaO	0.16
Fe_2O_3	0.24
Na_2O	0.10
K_2O	0.05
MgO	0.10
Al_2O_3	0.27
Loss of ignition (L.O.I.)	0.25

In this research, oleic acid (1000 g/t) was used in the flotation tests at pH 12.5, and the frother was methyl isobutyl carbinol (MIBC) (75 g/t). Sodium hydroxide (analytical grade) was used for pH regulation. The anionic flotation of quartz at pH 12.5 could be attributed to the presence of calcium ions and the activation of the quartz surface by this hydroxy ions (Ca^{2+}).

Flotation tests were carried out in a mechanical cell. An impeller diameter of 0.07 m was used for pulp agitation, and a square section cell with the length and the height of 0.12 and 0.1 m, respectively, was used. The impeller rotating speeds were 700, 900, 1100, and 1300 r/min, and the air flow rates were 15, 30, 45, and 75 L/h, respectively

2.1. Flotation response of quartz coarse particles

The Reynolds number (*Re*) is the ratio between inertial and viscous forces, the Froude number (*Fr*) is the ratio between inertial and gravity forces, and the Weber number (*We*) is the ratio between inertial and capillary forces. These dimensionless hydrodynamic parameters are calculated using the following equations [22].

$$Re = \left(ND^2\rho\right)/\mu_p \tag{1}$$

$$Fr = \left(N^2 D\right)/g \tag{2}$$

$$We = \left(N^2 D^3 \rho\right)/\gamma \tag{3}$$

where ρ is the pulp density, μ_p the pulp dynamic viscosity, g the gravity acceleration, γ the surface tension of the air/solution interface, N the impeller speed, and D the impeller diameter. Pulp viscosity is calculated by [23]

$$\mu_p = \mu_w (1-\phi)^{-2.5} \quad (4)$$

where μ_w is the water dynamic viscosity, and ϕ is the fraction of the pulp volume occupied by solids .

For different air flow rates, the influences of *Re*, *Fr*, and *We* on the recovery of quartz particles in four classes are illustrated in Fig 1. Quartz particles show a plateau of maximum recovery at *Re*=89800, *Fr*=2.4, and *We*=1588. For either more quiescent (*Re*<73500 and *Fr*<1.61) or more turbulent (*Re*>106200 and *Fr*>3.35) conditions, the flotation recovery decreases steadily.

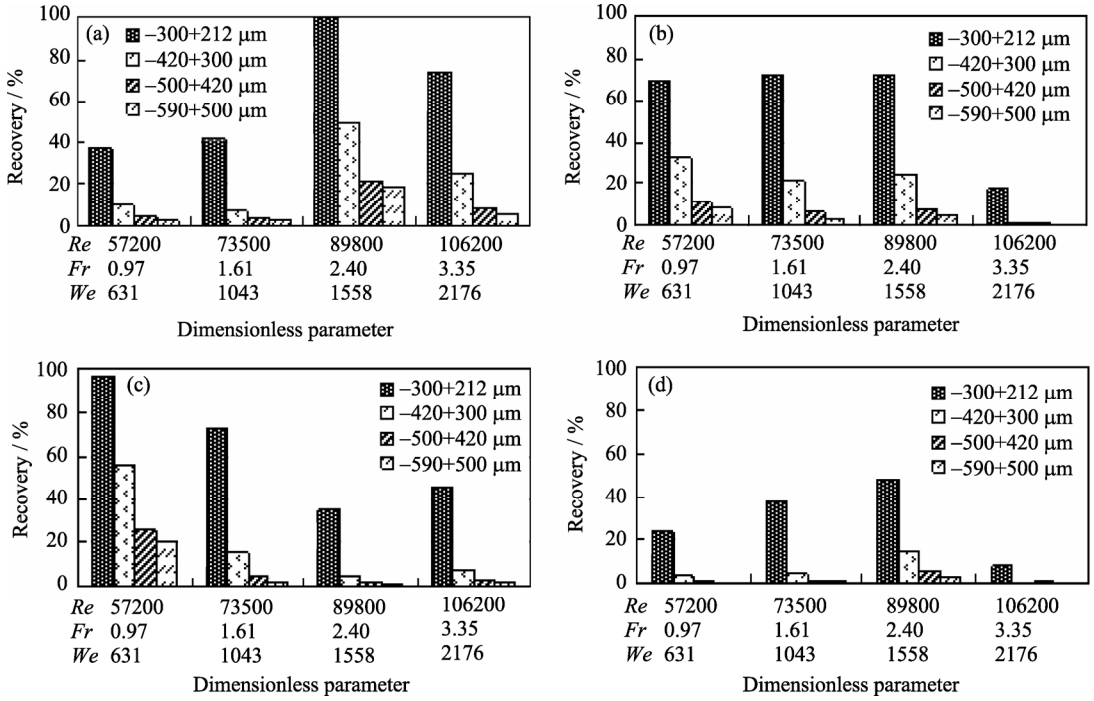

Fig. 1. Flotation response of quartz particles with dimensionless hydrodynamic parameters (*Re*, *Fr*, and *We*) at various air flow rates: (a) 15 L/h; (b) 30 L/h; (c) 45 L/h; (d) 75 L/h.

2.2. Bubble size distribution and rise velocity

In this research, the bubble size distribution and rise velocity were measured by a device similar to the McGill bubble viewer. It consists of a sampling tube attached to a viewing chamber with a window inclined 15° from vertical. The closed assembly was filled with water similar to that in the flotation cell to limit the changes in bubble environment during sampling. The tube was then immersed to the desired location below the froth. Bubbles rose into the viewing chamber and were imaged by a digital video camera. The bubbles slid up the inclined window and were illuminated from behind [24]. The mean bubble diameter adopted is the Sauter diameter (d_{32}), calculated by the following equation [25]:

$$d_{32} = \frac{\sum n_i d_i^3}{\sum n_i d_i^2} \quad (5)$$

where n is the number of bubbles, and d the bubble diameter. The parameters influencing the bubble Reynolds number (Re_b) are the bubble rise velocity and bubble diameter, as well as the density and dynamic viscosity of the surrounding fluid. The bubble Reynolds number is calculated by [26]

$$Re_b = V_b d_b \rho_f / \eta \quad (6)$$

where V_b is the bubble rise velocity, d_b the bubble diameter, η the fluid dynamic viscosity, and ρ_f the fluid density. As shown in Fig. 2 and Table 2, bubble diameter and bubble rise velocity distributions were measured under different conditions.

2.3. Collision probability

The probability (P) of a particle being collected by an air bubble in the pulp phase of a flotation cell can be given by [26]

$$P = P_c P_a (1 - P_d) \quad (7)$$

$$P_c = A\left(\frac{d_p}{d_b}\right)^n \quad (8)$$

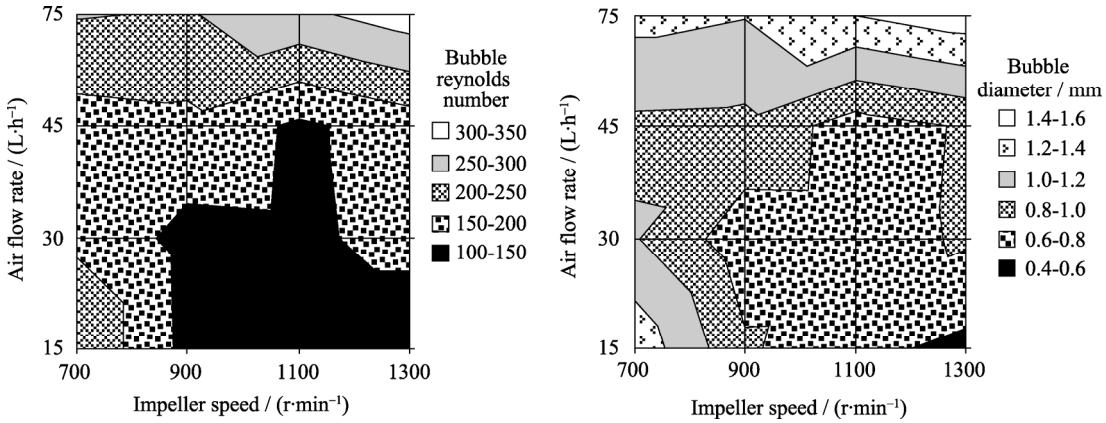

Fig. 2. Bubble Reynolds number (a) and bubble size (b) distributions under different conditions.

Table 2. Experimental results for quartz flotation in different operational conditions

Sample No.	*Fr*	*Re*	*We*	Particle size, d_p / μm	Air flow rate, Q / (L·h^{-1})	Bubble diameter, d_{32} / mm	Bubble rise velocity, V_p / (cm·s^{-1})	Collision probability, P_c / %	Recovery, R / %
1	3.35	106166.70	2175.94	256	30	0.83	18.47	7.00	8.44
2	0.97	57166.67	630.89	360	30	1.02	16.68	6.77	3.52
3	2.40	89833.33	1557.92	360	75	1.40	18.45	4.96	4.67
4	0.97	57166.67	630.89	360	45	0.96	16.73	10.43	9.82
5	1.61	73500.00	1042.91	360	30	0.68	17.69	14.57	4.11
6	0.97	57166.67	630.89	256	30	1.02	16.68	3.42	23.52
7	1.61	73500.00	1042.91	360	45	0.95	17.58	9.57	7.42
8	3.40	106166.70	2175.94	256	15	0.55	16.26	10.67	17.58
9	3.35	106166.70	2175.94	360	15	0.55	16.26	21.09	0.83
10	1.61	73500.00	1042.91	360	75	1.21	18.21	6.10	15.75
11	3.35	106166.70	2175.94	360	30	0.83	18.47	13.84	0.38
12	3.35	106166.70	2175.94	360	75	1.52	19.28	5.27	6.98
13	0.97	57166.67	630.89	545	15	1.34	16.58	11.03	8.28
14	0.97	57166.67	630.89	360	75	1.26	18.02	6.00	56.36
15	1.61	73500.00	1042.91	256	75	1.21	18.21	3.08	72.09
16	2.40	89833.33	1557.92	545	45	0.71	17.86	29.45	18.13
17	2.40	89833.33	1557.92	360	45	0.71	17.86	12.85	49.93
18	1.61	73500.00	1042.91	256	15	0.83	14.60	6.34	71.87
19	2.40	89833.33	1557.92	256	15	0.65	14.10	8.67	71.96
20	0.97	57166.670	630.89	256	15	1.34	16.58	2.43	69.01
21	3.35	106166.70	2175.94	256	45	0.82	18.98	6.50	74.24
22	0.97	57166.67	630.89	256	75	1.26	18.02	3.03	96.48
23	2.40	89833.33	1557.92	256	45	0.71	17.86	6.50	100.00
24	1.61	73500.00	1042.91	460	75	1.21	18.21	9.96	4.23
25	0.97	57166.67	630.89	256	45	0.96	16.73	5.28	37.36
26	0.97	57166.67	630.89	460	45	0.96	16.73	17.04	4.80
27	2.40	89833.33	1557.92	256	75	1.40	18.45	2.51	34.59
28	0.97	57166.67	630.89	460	30	1.02	16.68	11.05	0.87
29	2.40	89833.33	1557.92	460	75	1.40	18.45	8.10	1.90
30	1.61	73500.00	1042.91	460	30	0.68	17.69	23.79	0.93
31	2.40	89833.33	1557.92	360	30	0.69	17.90	18.15	14.62
32	1.61	73500.00	1042.91	460	45	0.95	17.58	15.63	4.06
33	1.61	73500.00	1042.91	360	15	0.83	14.60	12.54	21.04
34	1.61	73500.00	1042.91	256	30	0.68	17.69	7.37	38.02
35	1.61	73500.00	1042.91	460	15	0.83	14.60	20.48	6.03

(Continued)

Sample No.	*Fr*	*Re*	*We*	Particle size, d_p / μm	Air flow rate, Q / (L·h^{-1})	Bubble diameter, d_{32} / mm	Bubble rise velocity, V_p / (cm·s^{-1})	Collision probability, P_c / %	Recovery, R / %
36	1.61	73500.00	1042.91	256	45	0.95	17.58	4.84	41.67
37	2.40	89833.33	1557.92	460	15	0.65	14.10	27.98	7.09
38	2.40	89833.33	1557.92	360	15	0.65	14.10	17.14	23.91
39	3.35	106166.70	2175.94	460	75	1.52	19.28	8.61	2.30
40	0.97	57166.67	630.89	460	15	1.34	16.58	7.86	11.06
41	2.40	89833.33	1557.92	256	30	0.69	17.90	9.18	47.91
42	2.40	89833.33	1557.92	545	15	0.65	14.10	39.28	4.96
43	3.35	106166.70	2175.94	545	75	1.52	19.28	12.09	1.40
44	2.40	89833.33	1557.92	545	30	0.69	17.90	41.59	2.60
45	2.40	89833.33	1557.92	460	45	0.71	17.86	20.98	21.28
46	3.35	106166.70	2175.94	545	15	0.55	16.26	48.35	0.17
47	0.97	57166.67	630.89	360	15	1.34	16.58	4.81	32.51
48	3.35	106166.70	2175.94	545	30	0.83	18.47	31.73	0.10
49	0.97	57166.67	630.89	545	75	1.26	18.02	13.75	19.81
50	3.35	106166.70	2175.94	545	45	0.82	18.98	29.45	5.75
51	3.35	106166.70	2175.94	460	15	0.55	16.26	34.44	0.47
52	1.61	73500.00	1042.91	545	75	1.21	18.21	13.98	1.99
53	2.39	89833.33	1557.92	460	30	0.69	17.90	29.63	5.13
54	0.97	57166.67	630.89	545	45	0.96	16.73	23.91	2.44
55	3.35	106166.70	2175.94	460	30	0.83	18.47	22.60	1.33
56	2.40	89833.33	1557.92	545	75	1.40	18.45	11.36	0.88
57	0.97	57166.67	630.89	545	30	1.02	16.68	15.51	0.40
58	1.61	73500.00	1042.91	545	45	0.95	17.58	21.94	2.40
59	1.61	73500.00	1042.91	545	30	0.68	17.69	33.40	0.54
60	3.35	106166.70	2175.94	460	45	0.82	18.98	20.98	8.69
61	3.35	106166.70	2175.94	360	45	0.82	18.98	12.85	25.28
62	0.97	57166.67	630.89	460	75	1.26	18.02	9.80	26.11
63	1.61	73500.00	1042.91	545	15	0.83	14.60	28.74	3.01
64	3.35	106166.70	2175.94	256	75	1.52	19.28	2.67	45.67

where P_c is the probability of bubble particle collision, P_a the probability of adhesion, P_d the probability of detachment, d_p the diameter of the particle, d_b the diameter of the bubble, and A and n are the parameters varying with the Reynolds number. Table 3 gives these values for three different flow regimes considered, *i.e.*, Stokes, intermediate, and potential flows.

As shown in Table 2, the probability of collision is calculated for different particle sizes, air flow rates (15, 30, 45, and 75 L/h), and hydrodynamic dimensionless parameters (*Re*, *Fr*, and *We*) using the Stokes equation. Table 2 shows the laboratory results.

Table 3. Values of A and n in different flow conditions [26]

Flow condition	A	n
Stokes	2/3	2
Intermediate I	$\frac{3}{2}+\frac{4Re^{0.72}}{15}$	2
Intermediate II	$\frac{3}{2}\left[1+\frac{(3/16)Re}{1+0.249Re^{0.56}}\right]$	2
Potential	3	1

3. ANN procedure description

ANNs are composed of simple elements operating in parallel. These elements are inspired by biological nervous systems [27]. ANNs are able to produce a set of outputs for a given set of inputs according to some mapping relationships [28]. In nature, the network function is determined largely by the connections between elements. A neural network can be "trained" to perform a particular function by adjusting the values of the connections (weights) between elements [27]. During the training period, such relationships are coded into the network structure depending upon the network parameters [28]. Commonly, neural networks are adjusted or trained so that a particular input leads to a specific target output. The network is adjusted based on a com-

parison of the output and the target, until the network output matches the target [27].

The number of hidden layers and nodes may vary in different applications and depend on the user specifications. No specific technique is available to decide the optimum number, and it is usually found through a trial and error procedure [28].

The main advantages of neural networks over conventional regression analysis are freedom from linear supposition, a large number of freedom degrees, and more effective handling of nonlinear functional forms [29]. There are several classes of neural network architectures, classified according to their learning mechanisms. To develop a nonlinear ANN model of a system, feed-forward architecture, namely, MLP, is used most commonly. The feed-forward neural networks (FFNN) are the most popular architectures due to their structural flexibility, good representational capabilities, and availability of a large number of training algorithms [30]. This network consists of neurons arranged in layers in which every neuron is connected to all neurons of the next layer (a fully connected network). The structure of a feed-forward neural network is shown in Fig. 3.

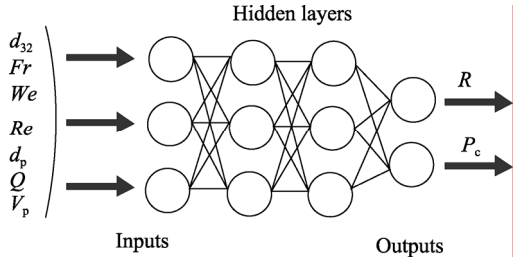

Fig. 3. Architecture of FANN.

The difference between the actual output and the network output is called error. There are several ways of measuring error, including normalized mean squared error (NMSE), mean absolute error (MAE), mean squared error (MSE), minimum absolute error, and maximum absolute error. MSE is the conventional measure for fitting data [31]. Hence, MSE is used to measure the error according to the following equation:

$$\mathrm{MSE}=\frac{1}{Q}\sum_{K=1}^{Q}(y_K-\hat{y})^2 \tag{9}$$

where Q is the number of observations in the data set, K the iteration number, y the network output, and $\hat{y}$ the actual output.

Therefore, in the present work, a multilayered feed-forward network with a back-propagation algorithm was used for the prediction of ash fusion temperature. The gradient descent optimization technique was employed to minimize the error [28].

4. Results and discussion

4.1. Regression

Linear regression estimates the coefficients of the linear equation, involving one or more independent variables which can best predict the value of the dependent variable. For example, you can try to predict a salesperson's total yearly sales (the dependent variable) from independent variables, such as age, education, and years of experience [32].

By a least squares mathematical method, the correlation coefficients of Fr, Re, We, d_p, Q, d_{32}, and V_p with recovery (R) are –0.14, –0.14, –0.14, –0.70, 0.11, 0.05, and –0.02, respectively, and with collision probability (P_c) are 0.29, 0.31, 0.29, 0.69, –0.41, –0.59, and –0.23, respectively. The best-fit equations for recovery and collision probability in terms of these parameters are as followed.

$$R=134.73-2.37Fr-6.2e^{-0.005}Re-0.165d_p+0.317Q-10d_{32}-2.366V_p,\ R^2=0.54 \tag{10}$$

$$P_c=13.961+3.832Fr-7.6e^{-0.005}Re+0.068d_p-0.001Q-18.886d_{32}-0.584V_p,\ R^2=0.87 \tag{11}$$

The differences between the predicted recovery and collision probability from Eqs. (10) and (11) and the actual measured values are shown in Figs. 4 and 5.

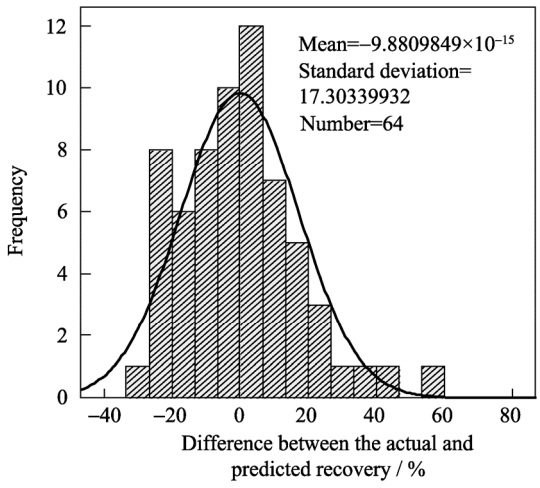

Fig. 4. Distribution of differences between the actual recovery and the estimated recovery from Eq. (10) for 64 samples.

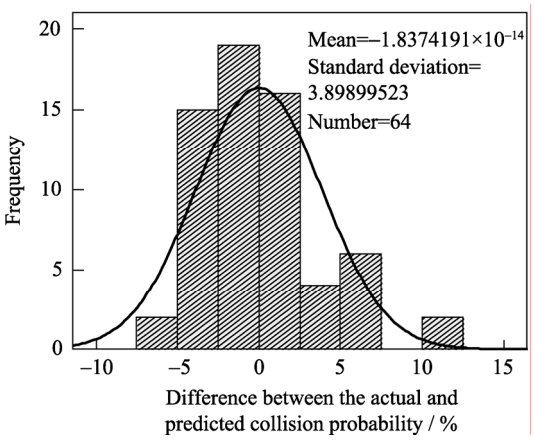

Fig. 5. Distribution of differences between the actual recovery and the estimated collision probability from Eq. (11) for 64 samples.

4.2. ANN results

According to Eqs. (10) and (11), the selected variables were used as input variables for the predictions of recovery and collision probability. After determining the number of input variables by statistical means, the most appropriate architecture for the network was determined. Several networks were created, trained, and tested. The number of layers, the optimum number of neurons per layer, and the transfer functions in the hidden layers were obtained by trial and error. In this study, a combined feed forward neural network (FANN) model was developed by using two hidden layers in MLP architecture and using the training of back-propagation (BP) algorithm. The BP algorithm first adjusted the weights connected to the output layer. Then, working backward toward the input layer, the algorithm adjusted the weights in each successive layer to reduce the errors at each level [30].

The 3-3-3-2 ANN model, which is recognized the effects in different operational conditions on the quartz flotation adequately, can predict both recovery and collision probability. The magnitudes of the data ranges are significantly different for each input as well as across the inputs. To ensure successful training, the data need to be prepared prior to training the neural network model [33]. To have a successful training process, the input and output data are preprocessed. In the present work, all inputs (before feeding to the network) and output data in training phase were preprocessed by normalizing the inputs and targets, so that they had the mean of 0 and the standard deviation of 1.

$$N_p = (A_p - A_{ps,\,mean}) / A_{p,\,std.} \quad (12)$$

where A_p is the actual parameter, $A_{ps,\,mean}$ the mean of the actual parameters, $A_{p,\,std.}$ the standard deviation of the actual parameter, and N_p the normalized parameter (input) [34]. The mean and standard deviation for preprocessing the input and output variables are shown in Table 4.

Table 4. Pre-processing parameters for ANN

Variable	Minimum	Maximum	Mean	Standard deviation
Fr	0.97	3.35	2.08	0.89
Re	57166.67	106166.70	81666.67	18405.58
We	630.89	2175.94	1351.91	582.67
d_p / μm	256.00	545.00	405.25	109.08
Q / (L·h^{-1})	15.00	75.00	41.25	22.36
d_{32} / mm	0.55	1.52	0.96	0.29
V_p / (cm·s^{-1})	14.10	19.28	17.34	1.41

A total of 64 datasets were used for the recovery and collision probability predictions by ANN, 54 datasets were used for training, and 10 sets were used for testing the network. The training process was stopped after 5000 epochs. In each epoch, the entire training set was presented to the network, case by case; errors were calculated and used to adjust the weights in the network using a sigmoid transfer function. This method was based on the BP error algorithm, which was an iterative supervised learning technique. A set of training examples was considered, and for each of these, the desired output of the MLP was known. [35]. The performance function used was the mean square error (MSE), which was the average squared error between the network predicted outputs and the target outputs. For the training data of the combined model, the MSE was 0.002.

The testing set, which actually tests how good the model is, shows that the model can estimate recoveries and collision probability quite satisfactorily. The correlation coefficient (R^2) values for testing sets are 0.98 in both recovery and collision probability predictions, as shown in Figs. 6 and 7.

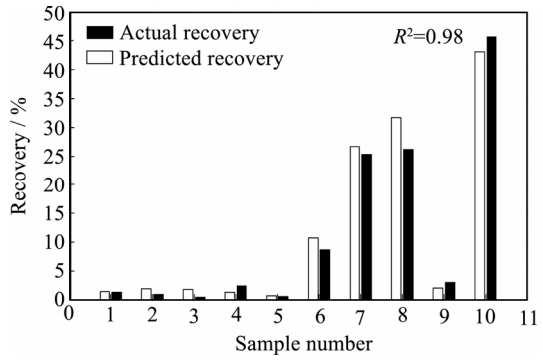

Fig. 6. Distributions of the actual recovery and the estimated recovery by neural network.

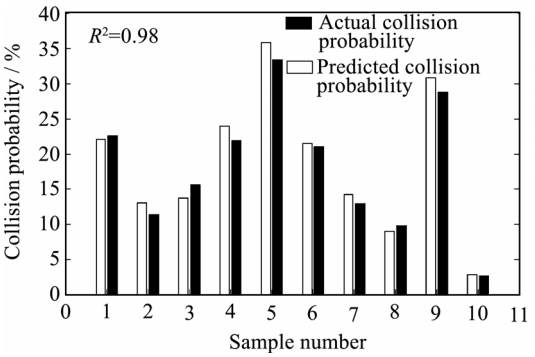

Fig. 7. Distributions of the actual collision probability and the estimated collision probability by neural network.

It is observed that simultaneous recovery and collision probabilities can be predicted satisfactorily using an ANN model.

5. Conclusions

(1) The effects of Froude number, Reynolds number, Weber number, particle size, air flow rate, bubble diameter, and bubble rise velocity on recovery and collision probability in the froth flotation of quartz were investigated in a laboratory flotation cell.

(2) Quartz particles showed a plateau of maximum recovery at Re=89800, Fr=2.4, and We=1588. For either more quiescent (Re<73500 and Fr<1.61) or more turbulent (Re>106200 and Fr>3.35) condition, flotation recovery decreased steadily. The maximum collision probability of around 48.35% was obtained at the impeller speed of 1100 r/min, air flow rate of 15 L/h, and particle size of 545 μm; and the minimum collision probability of around 2.43% was obtained at the impeller speed of 700 r/min, air flow rate of 15 L/h, and particle size of 256 μm.

(3) The measured laboratory data on the optimum parameters were compared to the simulation values by mathematical methods. Linear regression predicted recoveries and collision probabilities with correlation coefficients of 0.54 and 0.87, respectively, which are not significant according to the differences from the actual determined amount.

(4) Feed-forward artificial neural network procedures were used to improve the correlation coefficients. An FANN with 3-3-3-2 arrangement is capable of estimating both recovery and collision probability with high accuracy, simultaneously.

(5) In the ANN testing process, the model predicted both recovery and collision probability quite satisfactorily. The correlation coefficient (R^2) values for testing sets are 0.98 for both outputs.

(6) These studies on the dimensionless parameters in froth flotation constitute the new unexamined conditions, and ANNs have never been used to predict the amount of both recovery and collision probability.

(7) The method used and its related results can further be used as an expert system in froth flotation to optimize the process parameters and evaluate the parameter interactions for the expected recovery and collision probability without conducting new experiments in the laboratory.

Acknowledgements

The first author would like to thank D. Michael Laliberty.

References

[1] B.V. Derjaguin and S.S. Dukhin, Theory of flotation of small and medium-size particles, *Trans. Inst. Min. Metall.*, 70(1961), p.221.

[2] H.J. Schulze, *Physico-chemical Elementary Processes in Flotation: An Analysis from the Point of View of Colloid Science Including Process Engineering Considerations*, Elsevier, 1984, p.28.

[3] J. Ralston, D. Fornasiero, and R. Hayes, Bubble-particle attachment and detachment in flotation, *Int. J. Miner. Process.*, 56(1999), No.1-4, p.133.

[4] H. Schubert, On the turbulence-controlled microprocesses in flotation machines, *Int. J. Miner. Process.*, 56(1999), No.1-4, p.257.

[5] B.V. Derjaguin and S.S. Dukhin, Kinetic theory of the flotation of fine particles, [in] *Proceedings of the 13th International Mineral Processing Congress*, Warsaw, 1979, p.21.

[6] Y. Hu, G. Qiu, and D. Wang, The studies of carrier flotation of ultrafine wolframite, *Trans. Nonferrous Met. Soc. China*, 2(1994), p.44.

[7] F. Lafuma, K. Wong, and B. Cabane, Bridging of colloidal particles through adsorbed polymers, *J. Colloid Interface Sci.*, 143(1991), No.1, p.9.

[8] I.A. Valioulis and E.J. List, Collision efficiencies of diffusing spherical particles: hydrodynamic, van der Waals and electrostatic forces, *Adv. Colloid Interface Sci.*, 20(1984), p.1.

[9] L.J. Warren, Ultrafine particles in flotation, [in] *Principles of Mineral Flotation*, Victoria, 1984, p.185.

[10] R. Crawford and J. Ralston, The influence of particle size and contact angle in mineral flotation, *Int. J. Miner. Process.*, 23(1988), p.1.

[11] P.D. Wasserman, *Neural Computing: Theory and Practice*, Van Nostrant Reinhold, New York, 1989.

[12] R.T. Beale and H. Adam, *Neural Computing: An Introduction*, Van Nostrant Reinhold, Bristol, 1990.

[13] C. Acharya, S. Mohanty, L.B. Sukla, and V.N. Misra, Prediction of sulphur removal with Acidithiobacillus sp. using artificial neural networks, *Ecol. Modell.*, 190(2006), p.223.

[14] E. Jorjani, S. Chehreh Chelgani, and Sh. Mesroghli, Prediction of microbial desulfurization of coal using artificial neural networks, *Miner. Eng.*, 20(2007), p.1285.

[15] E. Jorjani, S. Chehreh Chelgani, and Sh. Mesroghli, Application of artificial neural networks to predict chemical desulfurization of Tabas coal, *Fuel*, 87(2008), p.2727.

[16] S. Chehreh Chelgani and E. Jorjani, Artificial neural network prediction of Al_2O_3 leaching recovery in the Bayer process at the Jajarm alumina plant (Iran), *Hydrometallurgy*, 97(2009), p.105.

[17] B. Venkoba Raoa and S.J. Gopalakrishna, Hardgrove grindability index prediction using support vector regression, *Int. J. Miner. Process.*, 91(2009), No.1-2, p.55.

[18] S. Chehreh Chelgani, J.C. Hower, E. Jorjani, *et al.*, Prediction of coal grindability based on petrography, proximate and ultimate analysis using multiple regression and artificial neural network models, *Fuel Process. Technol.*, 89(2008), p.13.

[19] E.C. Cilek, Application of neural networks to predict locked cycle flotation test results, *Miner. Eng.*, 15(2002), p.1095.

[20] J. Labidi, M.A. Pèlach, X. Turon, and P. Mutjé, Predicting flotation efficiency using neural networks, *Chem. Eng. Process.*, 46(2007), p.314.

[21] P. Clifford, M. Lloyd, and P. Zhang, Technology research improves phosphate economics, *Miner. Eng.*, 98(1998), p.46.

[22] W.J. Rodrigues, L.S.L. Filho, and E.A. Masini, Hydrodynamic dimensionless parameters and their Influence on flotation performance of coarse particles, *Miner. Eng.*, 14(2001), p.1047

[23] R. Roscoe, The viscosity of suspensions of rigid spheres, *Br. J. Appl. Phys.*, 3(1952), p.267.

[24] E.H. Girgin, S. Do, C.O. Gomez, and J.A. Finch, Bubble size as a function of impeller speed in a self-aeration laboratory flotation cell, *Miner. Eng.*, 19(2006), p.201.

[25] R.T. Rodrigues and J. Rubio, New basis for measuring the size distribution of bubbles, *Miner. Eng.*, 16(2003), p.757.

[26] R.H. Yoon, The role of hydrodynamic and surface forces in bubble-particle interaction, *Int. J. Miner. Process.*, 58(2000), No.1-4, p.129.

[27] M.A. Hakeem, M. Kamil, and I. Arman, Prediction of temperature profiles using artificial neural networks in a vertical thermosiphon reboiler, *Appl. Therm. Eng.*, 28(2008), p.1572.

[28] A. Afkhami, M. Abbasi-Tarighat, and M. Bahramb, Artificial neural networks for determination of enantiomeric composition of α-phenylglycine using UV spectra of cyclodextrin host-guest complexes. Comparison of feed-forward and radial basis function networks, *Talanta*, 75(2008), p.91.

[29] F.F. Farshad, J.D. Garber, and J.N. Lorde, Predicting temperature profiles in producing oil wells using artificial neural networks, *Eng. Comput.*, 17(2000), p.735.

[30] E. Razmi-Rad, B. Ghanbarzadeh, S.M. Mousavi, *et al.*, Prediction of rheological properties of Iranian bread dough from chemical composition of wheat flour by using artificial neural networks, *J. Food Eng.*, 81(2007), p.728.

[31] A. Alonso-Rodriguez, Forecasting economic magnitudes with neural network models, *Int. Adv. Econ. Res.*, 5(1999), No.4, p.496.

[32] S. Landau and S.E. Brian, *A Handbook of Statistical Analyses Using SPSS*, Chapman Hall/Crc, New York, 2004, p.113.

[33] K. Smith, *Neural Networks in Business: Techniques and Applications*, Idea Group Publishing, Hershey, 2002.

[34] H. Demuth and M. Beale, *Neural Network Toolbox for Use with MATLAB*, The Mathworks Inc., Natick, 2002, p.154.

[35] C. Aldrich, *Exploratory Analysis of Metallurgical Process Data with Neural Networks and Related Methods*, Elsevier, Amsterdam, 2002, p.5.